Polymer Chemistry

Synthesis, postmodification and fluorescent properties of reduction-cleavable core-couplable miktoarm stars with a branched core

ARTICLE TYPE

Synthesis, postmodification and fluorescent properties of reduction-cleavable core-couplable miktoarm stars with a branched core†

Cangxia Li, Huanhuan Liu, Dandan Tang and Youliang Zhao*

Novel amphiphilic $(PEG)_m(PCL)_n$ (m ≈ n ≈ 23) miktoarm stars with a disulfide-linked epoxy-functionalized branched core were controllably synthesized via three step reactions comprising self-condensing vinyl polymerization via reversible addition−fragmentation chain transfer, epoxy-carboxyl coupling reaction and ring-opening polymerization. The star copolymers were characterized by ^{1}H NMR
10 spectra, GPC-MALLS, DSC and reduction-triggered degradation. Postpolymerization modification via epoxy-carboxyl/phenol coupling reactions allowed attaching dual-reactive functionalities including coumarin, alkyne and alkyl bromide onto the branched core. In water and THF/water mixtures, coumarin-modified star copolymer could aggregate into some intriguing morphologies including hyperbranched micelles and large vesicles due to the influence of solvent polarity on aggregation behaviors. Owing to the
15 differences in isolation of fluorophores from solvent and restricted molecular motion, coumarin-functionalized star exhibited adjustable fluorescent properties in water and THF/water mixtures, and its aqueous solution had a maximum quantum yield (Φ_F = 44.2%). The solutions of star copolymer and its reduction-cleaved copolymer were of different hydrodynamic diameters, and the $\Phi_F(star)/\Phi_F(cleaved copolymer)$ values were 1.85 (in THF), 3.00 (in water) and ranged between 1.29 and 2.58 in THF/water
20 mixtures, revealing the aggregation behaviors and fluorescent properties were strongly dependent on polymeric architecture, location of fluorophores and solvent polarity. Our study affords a versatile method to construct functional miktoarm stars with a multi-reactive branched core, and coumarin-functionalized star copolymer may have a great potential as solvent polarity and reduction dual-sensitive imaging materials in "green" ink, coating and nanocarriers for biomedical applications.

25 Synthesis and properties of functional multiarm and miktoarm star polymers have attracted extensive attention due to their unique physicochemical properties and multipurpose applications.[1−10] As compared with their linear analogues, star polymers are liable to exhibit distinctly different bulk, solution
30 and interface properties originating from their increasing compact structures and end groups. Owing to their branched architectures and heterophase structures, miktoarm stars with arms more than one chemical composition can perform phase separation at the molecular level and self-assemble into multiscale nano-ordered
35 suprastructures and supramolecular assemblies, and they are expected to hold great promise as next-generation multiphase polymer materials.[11−21] As well documented, the precise structure is essential to elucidate the internal correlations among structure, property and application of star polymers. Tremendous progress
40 in living ionic polymerization and reversible deactivation radical polymerization has turned controlled synthesis of star polymers into reality, and some approaches involving "arm first",[22−24] "core first",[25−27] "coupling onto"[28,29] and combinatorial methods[30−33] have paved ways for facile synthesis and versatile
45 applications towards functional materials.

Generally speaking, star polymers are composed of a central core and polymer arms, in which the core can be small molecule, linear chain,[34−36] dendrimer[26,27,37] and hyperbranched polymer.[38−41] Among them, star polymers with a branched core
50 have attracted increasing interest due to the ability for versatile postpolymerization and postfunctionalization of the hyperbranched scaffold.[38−41] As compared with functional dendrimer constructed via iterative methods comprising multi-step syntheses, segmented hyperbranched polymer (SHP) can be
55 efficiently achieved via one-pot self-condensing vinyl polymerization (SCVP)[42] based on controlled radical polymerization (CRP) such as atom transfer radical polymerization (ATRP)[43−48] and reversible addition−fragmentation chain transfer (RAFT)[49−54] polymerization. The
60 CRP SCVP techniques allow controlled synthesis of hyperbranched polymers with relatively low polydispersity, variable molecular parameters, and on-demand functionalities, which can act as ideal scaffolds to generate the target star polymers via postpolymerization modification. Moreover, the
65 great potential in synthesis of miktoarm stars and other complex architectures can be further enhanced as highly efficient linking reaction is applied.[40,41] For instance, some ion-bearing A_mB_n-type (A and B can be any types of polymer segments in theory) miktoarm stars with a branched core comprising *N,N*-
70 dimethylaminoethyl methacrylate (DMA) units have been

constructed by us via two or three step reactions based on SCVP, RAFT process and Menschutkin reaction.[40] Although this approach allows facile synthesis of the target stars with variable arm number and chemical composition, it still has some limitations such as reduced solubility and unsatisfactory grafting efficiency, and thus it is urgent to explore more ideal approaches for the syntheis.

On the other hand, the incorporation of organic dyes such as pyrene, tetraphenylethylene and coumarin into polymeric architectures has attracted much attention due to their potential applications in solution-based fluorescent sensors, optical imaging, light-harvesting and photochromic materials, and organic electronic devices.[55–63] As the fluorescent moieties were introduced into star and branched architectures, they may exhibit distinct fluorescent properties due to the changes in microenvironments bearing dye moieties, polymer segments and solvent. Among them, coumarin is a natural and biocompatible substance that can undergo reversible dimerization and depolymerization under UV light with different wavelengths, and thus coumarin-containing polymers can act as promising precursors for formation of reversible photo-cross-linkable micelles with potential biomedical applications.[64–67] Some linear, dendritic-linear block copolymer,[68] star[69,70] and dendrigraft[71,72] polymers with coumarin functionalities have been synthesized and used to reveal structure-property relationship. However, no examples of coumarin-bearing miktoarm stars have been achieved thus far.

Herein, we reported on synthesis and properties of multicleavable core-couplable $(PEG)_m(PCL)_n$-type (m and n denote the arm number) star copolymers with a disulfide-linked branched core (Scheme 1). The miktoarm stars were synthesized by three step reactions, namely, RAFT copolymerization of 2-((2-(acryloyloxy)ethyl)disulfanyl)ethyl 4-cyano-4-(phenylcarbono thioylthio)pentanoate (ACP) and glycidyl methacrylate (GMA) afforded hyperbranched PGMA, a subsequent epoxy-carboxyl coupling reaction between PGMA and carboxyl-terminated poly(ethylene glycol) (PEG-COOH) gave multiarm star PEG with a branched core, and the newly generated hydroxyl moieties were further used to initiate ring-opening polymerization (ROP) of ε-caprolactone (CL) to generate the target stars. On this basis, postpolymerization modification was conducted to attach some reactive moieties such as coumarin, alkyne and alkyl bromide onto the branched core. Additionally, aggregation behaviors and fluorescent properties of coumarin-functionalized star before and after reduction were investigated.

The resultant miktoarm stars have some features. The presence of disulfide linkages in each branching point enables reduction-triggered degradation and topological transformation, and the remaining GMA units allow straightforward and sequential postpolymerization modifications to construct heterofunctional materials, in which the incorporation of various functionalities further enhances the potential utility in the arena of nanoreactors, fluorescence markers, and drug delivery applications. Moreover, disulfide-linked multicoumarin-functionalized miktoarm stars are sensitive to reduction and light irradiation and can act as model samples to investigate the effects of polymeric architecture and location of fluorophores on physicochemical properties. To the best of our knowledge, this is the first report on facile synthesis

of functional miktoarm stars with PEG and PCL segments and a dual- and multi-reactive branched core. The versatile methodology is suitable for rapid construction of multicleavable A_mB_n-type miktoarm stars with on-demand chemical composition, arm number and cleavable linkage.

Experimental section

Materials

All solvents, monomers, and other chemicals were purchased from Sigma-Aldrich unless otherwise stated. ε-Caprolactone (CL, 99%) was distilled from calcium hydride under reduced pressure. Glycidyl methacrylate (GMA, 99%) was passed through a basic alumina column to remove the inhibitor before use. 2,2′-Azobis(isobutyronitrile) (99%, AIBN) was recrystallized twice from ethanol. Monomethoxy poly(ethylene glycol) (MPEG, M_n = 2000) was dried by azeotropic distillation. 4-Cyanopentanoic acid dithiobenzoate (4-CPDB),[73] 2-((2-hydroxyethyl)disulfanyl)ethyl 4-cyano-4-(phenylcarbonothioylthio)pentanoate,[74] 2-((2-(acryloyl oxy)ethyl)disulfanyl)ethyl 4-cyano-4-(phenylcarbonothioylthio) pentanoate (ACP),[52] carboxyl-terminated poly(ethylene glycol) (MPEG-COOH, $M_{n,NMR}$ = 2100, $M_{n,GPC}$ = 2360, PDI = 1.05),[75] and 4-oxo-4-(prop-2-yn-1-yloxy)butanoic acid[76] were synthesized and purified according to literature procedures. N,N'-Dicyclohexylcarbodiimide (95%, DCC), 4-dimethylamino pyridine (98%, DMAP), and tetrabutyl ammonium bromide (99%, TBAB) were purchased from Sinopharm Chemical Reagent Co., Ltd. and used as received. DL-dithiothreitol (DTT, 99%, Merck), doxorubicin hydrochloride (> 99%, Zhejiang Hisun Pharmaceutical Co, Ltd.), $Sn(Oct)_2$ (99%), 2-bromopropionic acid (98%, Aladdin) and 7-hydroxy-4-methylcoumarin (98%, Aladdin) were used as received. Dichloromethane (DCM), dioxane, tetrahydrofuran (THF), dimethyl sulfoxide (DMSO), anisole and N,N-dimethylformamide (DMF) were purified according to standard procedures.

Synthesis of hyperbranched PGMA by RAFT self-condensing vinyl copolymerization (SCVP)

To a Schlenk tube were added ACP (0.940 g, 2.0 mmol), GMA (5.69 g, 40 mmol), AIBN (65.6 mg, 0.40 mmol) were added, and dry dioxane was added until the total volume was 40 mL. The contents were degassed with bubbled nitrogen for 30 min, and then the polymerization was conducted at 70 °C for 10 h. After precipitation into cold methanol and vacuum drying, 3.50 g (52.8% total monomer conversion) of hyperbranched PGMA was obtained. Number-average molecular weight and polydispersity determined by GPC-MALLS were M_n = 17300 and PDI = 1.44. Based on GPC-MALLS and NMR analyses, its number-average CTA functionality (f_{CTA}) was determined to be 5.2, and each dithiobenzoate moiety corresponded to 20.1 GMA units.

Hyperbranched PGMA: ^{1}H NMR (CDCl₃): δ 7.95, 7.55, 7.40 (m, PhH), 6.47 and 5.89 (m, CH_2=CH), 6.15 (m, CH₂=CH), 4.43 (m, COOCH_2CH₂S), 4.32 and 3.81 (each s, COOCH_2 of GMA unit), 3.24 (m, CH of GMA unit), 2.92 (m, CH_2S), 2.85 and 2.64 (each s, CH_2O of GMA unit), 0.6-2.6 (m, other CH, CH_2 and CH_3 originating from CTA and GMA unit). FT-IR (KBr): 3430, 3069, 2999, 2936, 1731, 1634, 1485, 1450, 1385, 1343, 1257, 1236, 1172, 1150, 1134, 1078, 994, 907, 847, 759, 691 cm⁻¹.
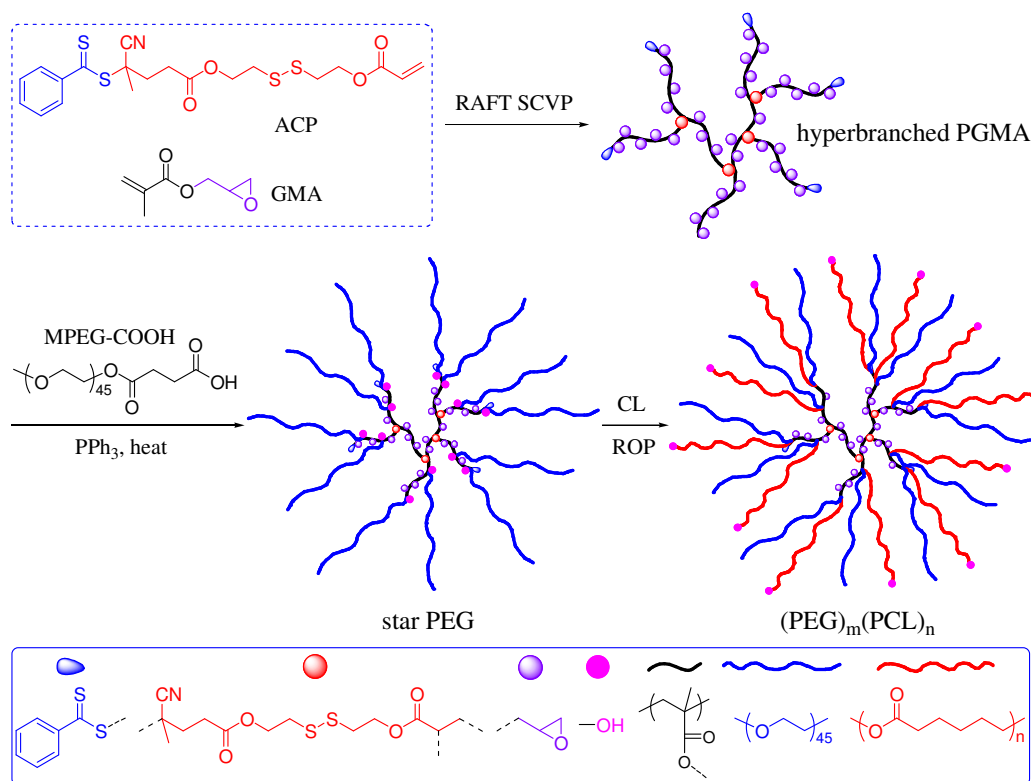
Scheme 1 Synthesis of $(PEG)_m(PCL)_n$ star copolymers with a disulfide and epoxy dual-reactive branched core by combination of RAFT SCVP, carboxyl-epoxy coupling reaction and ROP

5

Synthesis of multiarm star PEG by epoxy-carboxyl coupling reaction

Hyperbranched PGMA (1.65 g, 10.0 mmol of epoxy functionality), MPEG-COOH (10.5 g, 5.0 mmol), PPh₃ (0.13 g, 0.5 mmol), and 81 mL of DMF were added to a round flask. The contents were degassed with bubbled N₂ and reacted at 110 °C for 20 h. The polymerization solution was precipitated into diethyl ether, and the crude product was collected and partitioned between DCM and deionized water. The organic layer was washed with water twice, and the polymer-based aqueous solution was combined and subjected to dialysis (MWCO 10 kDa). Lyophilization gave 6.22 g of star PEG with PGMA core. GPC-MALLS and ^{1}H NMR analyses: M_n = 65700, PDI = 1.26, and $M_{n,NMR}$ = 66500.

Star PEG: ^{1}H NMR (CDCl₃): δ 7.3-8.0 (m, PhH), 6.1-6.5 (m, CH_2=CH), 3.8-4.5 (m, CHOH and COOCH_2), 3.65 (s, CH_2O of PEG), 3.38 (s, CH_3O of PEG), 3.27 (m, CH of GMA unit), 2.5-3.0 (m, CH_2S, CH_2O of GMA unit, and OCOCH_2CH_2COO connecting with PEG), 0.6-2.4 (m, other CH, CH_2 and CH_3 originating from CTA and GMA unit). FT-IR (KBr): 3423, 2879, 1732, 1649, 1468, 1384, 1351, 1282, 1250, 1199, 1107, 1042, 952, 844, 746, 686 cm^{-1}.

Synthesis of A_mB_n (A = PEG, B = PCL, m ≈ n) star copolymers by CL polymerization

Ring-opening polymerization using star PEG as a macroinitiator was used to grow PCL grafts. In a typical experiment (run 3 of Table 1), to a glass tube under nitrogen were added star PEG (0.580 g, 0.20 mmol of OH functionality), CL (0.457 g, 4.0 mmol) and Sn(Oct)₂ (16.2 mg, 0.04 mmol), and dry toluene was added until the total volume was 2.0 mL. After three freeze-evacuate-thaw cycles, the tube was sealed under vacuum and placed in an oil bath thermostated at 110 °C. The polymerization was stopped after 20 h, and the solution was precipitated into a large amount of hexane to isolate the polymer. After filtration and drying in vacuo, 0.978 g (87.1% conversion) of $(PEG)_m(PCL)_n$ star copolymer (S1) was obtained. GPC-MALLS and ^{1}H NMR analyses: M_n = 108000, PDI = 1.18, and $M_{n,NMR}$ = 112000. Other $(PEG)_m(PCL)_n$ stars (S2 and S3) were synthesized and purified according to similar procedures.

$(PEG)_m(PCL)_n$ star: ^{1}H NMR (CDCl₃): δ 7.3-8.0 (m, PhH), 6.1-6.5 (m, CH_2=CH), 3.8-4.5 (m, CHOH and COOCH_2), 3.65 (s, CH_2O of PEG), 3.38 (s, CH_3O of PEG), 3.27 (m, CH of GMA unit), 2.5-3.0 (m, CH_2S, CH_2O of GMA unit, and CH_2COO), 0.6-2.4 (m, other CH, CH_2 and CH_3 originating from CTA, GMA unit and PCL). FT-IR (KBr): 3438, 2945, 2868, 1726, 1649, 1472, 1419, 1398, 1368, 1296, 1244, 1191, 1107, 1048, 959, 841, 732 cm^{-1}.

Postpolymerization modification of $(PEG)_m(PCL)_n$ star

In a typical run, S3 star (100 mg), 7-hydroxy-4-methylcoumarin (30 mg), TBAB (10 mg), and 1.0 mL of DMSO were added to a glass tube under nitrogen, and the contents were reacted at 120 °C for 20 h. The solution was concentrated and precipitated into ethanol / water mixture, and the product was isolated by centrifugation. After vacuum drying, 110 mg of coumarin-functionalized $(PEG)_m(PCL)_n$ star (denoted as S4) was obtained.

For the synthesis of other samples, epoxy-carboxyl reaction between S3 and 4-oxo-4-(prop-2-yn-1-yloxy)butanoic acid or 2-bromopropionic acid was performed in anisole at 100 °C for 30 h, and the resultant star copolymers were purified by precipitation.

Coumarin-functionalized star (S4): ^{1}H NMR (CDCl₃): δ 7.3-8.0 (m, Ph*H* and Ar*H* of coumarin), 6.92 (s, Ar*H* of coumarin), 6.0-6.5 (m, C*H*₂=C*H* and C*H*COO of coumarin), 3.8-4.5 (m, C*H*OH and COOC*H*₂), 3.65 (s, C*H*₂O of PEG), 3.38 (s, C*H*₃O of PEG), 3.27 (m, C*H* of GMA unit), 2.5-3.0 (m, C*H*₂S, C*H*₂O of GMA unit, and C*H*₂COO), 0.6-2.4 (m, other C*H*, C*H*₂ and C*H*₃ originating from CTA, GMA unit, PCL, and coumarin).

Alkyne-functionalized star (S5): ^{1}H NMR (CDCl₃): δ 7.3-8.0 (m, Ph*H*), 6.1-6.5 (m, C*H*₂=C*H*), 4.70 (s, C*H*₂C≡CH), 3.8-4.5 (m, C*H*OH and COOC*H*₂), 3.65 (s, C*H*₂O of PEG), 3.38 (s, C*H*₃O of PEG), 3.27 (m, C*H* of GMA unit), 2.5-3.0 (m, C*H*₂S, C*H*₂O of GMA unit, and C*H*₂COO), 2.50 (s, C*H*₂C≡C*H*), 0.6-2.4 (m, other C*H*, C*H*₂ and C*H*₃ originating from CTA, GMA unit and PCL).

Bromide-functionalized star (S6): ^{1}H NMR (CDCl₃): δ 7.3-8.0 (m, Ph*H*), 6.1-6.5 (m, C*H*₂=C*H*), 3.8-4.8 (m, C*H*Br, C*H*OH and COOC*H*₂), 3.65 (s, C*H*₂O of PEG), 3.38 (s, C*H*₃O of PEG), 3.27 (m, C*H* of GMA unit), 2.5-3.0 (m, C*H*₂S, C*H*₂O of GMA unit, and C*H*₂COO), 0.6-2.4 (m, other C*H*, C*H*₂ and C*H*₃ originating from CTA, OCOCHBrC*H*₃, GMA unit and PCL).

Reduction-triggered degradation of star copolymer

Under nitrogen, S2 star (20 mg) was dissolved in 1.0 mL of THF, and followed by addition of about 3.0 μL of Bu₃P. After stirring at 25 °C for 16 h, the mixture was diluted with THF and subjected to GPC analysis. Molecular weight and polydispersity of cleaved copolymer were M_n = 29800, PDI = 1.30. According to a similar procedure, cleaved S4 (M_n = 50600, PDI = 1.36) was obtained by reduction-triggered degradation of S4 star (M_n = 242000, PDI = 1.16).

Characterization

Gel permeation chromatography with multiple angle laser scattering detection (GPC-MALLS) systems was used to determine absolute number-average molecular weight (M_n), polydispersity (PDI) and solution viscosity of various copolymers. GPC was conducted in THF at 35 °C with a flow rate of 1.0 mL min⁻¹. Three TSK-GEL H-type columns (pore size 15, 30 and 200 Å, with molecular weight range of 100–1000, 300–20000 and 5000–400000 g mol⁻¹, respectively) with 5 μm bead size were used. Detection consisted of a RI detector (Optilab rEX), a multi-angle (14-145°) laser light scattering (MALLS) detector (DAWN HELEOS) with the He-Ne light wave length at 658.0 nm, and on-line viscosity detector (ViscoStar). The refractive index increment d*n*/d*c* for samples were measured off-line by Optilab rEX refractive index detector (λ = 658 nm) at 25 °C using a series of different concentration solutions. Data were collected and processed by use of ASTRA software from Wyatt Technology, and molecular weights were determined by the triple detection method. ^{1}H NMR spectra (400 MHz) were recorded on a Varian spectrometer at 25 °C using CDCl₃ as a solvent. Fourier Transform Infrared (FT-IR) spectra were recorded on a Perkin-Elmer 2000 spectrometer using KBr discs. Differential scanning calorimetry (DSC) analysis was performed under a nitrogen atmosphere on Q200 DSC (TA Instruments - Waters LLC) with a

heating rate of 10 °C min⁻¹. UV-vis absorption spectra were recorded on a Shimadzu UV-3150 spectrophotometer, fluorescence spectroscopy was recorded at 25 °C on a FLS920 fluorescence spectrometer, and the fluorescence quantum yield (Φ_F) was determined by using quinine sulfate in 0.05 M H₂SO₄ (Φ_F = 54.6%) as reference standard. Dynamic light scattering (DLS) measurements were carried out at 25 °C using Zetasizer Nano-ZS from Malvern Instruments equipped with a 633 nm He–Ne laser using back-scattering detection.
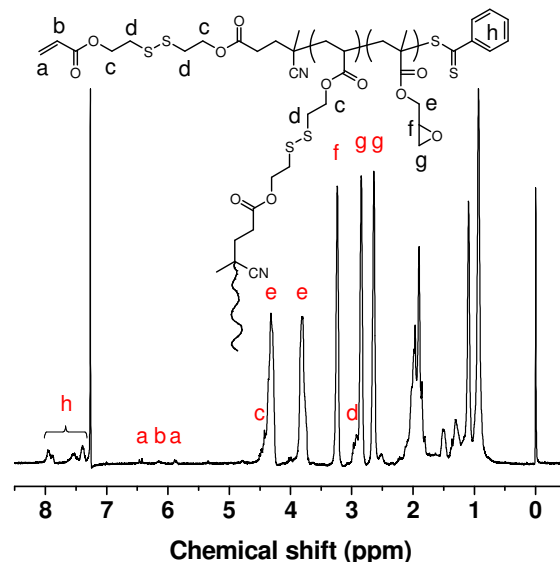

Fig. 1 ^{1}H NMR spectrum of hyperbranched PGMA (The wavy line denotes PGMA branches).

Results and discussion

Synthesis of hyperbranched PGMA

RAFT SCVP allowed controlled synthesis of the target branched copolymers with variable degree of branching (DB), polydispersity (PDI) and CTA functionality (F) under optimized conditions.[39–41] RAFT copolymerization of ACP and GMA was performed to generate hyperbranched PGMA with controlled number of dithiobenzoate moieties, couplable epoxy groups and cleavable disulfide linkage in each branching point.

As the copolymerization ([GMA]₀:[ACP]₀:[AIBN]₀ = 20:1:0.2, [M]₀ = 1.0 mol L⁻¹) was performed in dioxane at 70 °C for 10 h, hyperbranched PGMA was obtained in 52.8% conversion (run 1 of Table 1). In ^{1}H NMR spectrum (Fig. 1), the signals of aromatic and remaining vinyl protons originating from ACP appeared at δ 7.95, 7.55, 7.40 (Ph*H*), and 6.47, 6.15, 5.89 (C*H*₂=C*H*), the protons beside disulfide linkages remained at δ 4.43 (COOC*H*₂CH₂S) and 2.92 (C*H*₂S), and characteristic signals of GMA units were noted at δ 4.32, 3.81 (COOC*H*₂), 3.24 (C*H*O of epoxy), 2.85 and 2.64 (C*H*₂O of epoxy). The number-average molecular weight and polydispersity were determined to be M_n = 17300 and PDI = 1.44 by GPC-MALLS, and the resultant PGMA exhibited monomodal distribution in GPC trace (Fig. 2). Based

Table 1 Molecular weight, polydispersity, and DSC results of hyperbranched PGMA (run 1), star PEG (run 2), and $(PEG)_m(PCL)_n$ (m ≈ n ≈ 23) star copolymers (runs 3-5)[a]

run	sample	$M_{n,th}$ (kDa)[b]	M_n (kDa)[c]	PDI[c]	dn/dc	$M_{n,NMR}$ (kDa)[d]	$f_{w,PEG}$[d]	$f_{w,PCL}$[d]	T_g (°C)[e]	T_m (°C)[e]	ΔH (J g^{-1})[e]
1	PGMA	—	17.3	1.44	0.0807	—	—	—	56.9	—	—
2	$(PEG)_m(OH)_m$	66.0	65.7	1.26	0.0862	—	0.737	0	—	52.5	89.7
3	S1	112	108	1.18	0.0846	111	0.448	0.392	-52.0	49.3	79.2
4	S2	162	150	1.13	0.0835	155	0.323	0.562	-50.2	46.3, 51.0	58.3
5	S3	218	228	1.14	0.0820	221	0.212	0.712	-49.8	40.9, 54.3	48.1

[a] Reaction conditions: $[GMA]_0:[ACP]_0:[AIBN]_0$ = 20:1:0.2, $[M]_0$ = 1.0 mol L^{-1}, in dioxane at 70 °C for 10 h (run 1); $[PEG\text{-}COOH]_0$: $[GMA]_0:[PPh_3]_0$ = 10:20:0.1, $W_{polymer}$:V_{DMF} = 0.15 g mL^{-1}, at 110 °C for 20 h (run 2) ; $[CL]_0:[OH]_0:[Sn(Oct)_2]_0$ = x:1:0.2, x = 20 (run 3), 40 (run 4) or 60 (run 5), $[M]_0$ = 2.0 mol L^{-1}, in toluene at 110 °C for 20 h (runs 3-5). [b] Theoretical molecular weight calculated from M_n of macroinitiator and monomer conversion. [c] Number-average molecular weight (M_n) and polydispersity (PDI) determined by GPC-MALLS. [d] Number-average molecular weight ($M_{n,NMR}$) and weight percent (f_w) of polymer segments determined by ^{1}H NMR analysis. [e] Glass transition temperature (T_g), maximum melting peak (T_m), and enthalphy (ΔH) determined by DSC.
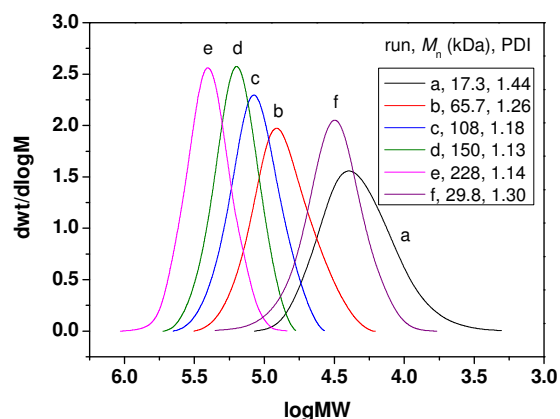
Fig. 2 GPC traces of hyperbranched PGMA (a), star PEG (b), $(PEG)_m(PCL)_n$ star copolymers (c, S1; d, S2; e, S3) and cleaved copolymer obtained after Bu$_3$P triggered reduction of S2 star (f).

on the equation $F_n = M_n \times I_{7.95}/(MW_{ACP} \times I_{7.95} + 2MW_{GMA} \times I_{3.24})$, number-average CTA functionality per hyperbranched PGMA was deduced to be 5.2, in which MW_{ACP} and MW_{GMA} were molecular weights of ACP and GMA. By comparing the integrated signal areas at 3.24 and 7.95 ppm, the molar ratio of GMA to dithiobenzoate was determined to be 20.1 (R = $2I_{3.24}/I_{7.95}$), and thus each hyperbranched PGMA comprised about 105 GMA units. By assuming that no CTA functionality was lost during RAFT SCVP, the repeat unit per branch (RB) was calculated as 11.1 using the equation RB = $(I_{3.24} + I_{7.95})/I_{7.95}$. Owing to the high reactivity of epoxy groups, the resultant hyperbranched PGMA afforded a versatile platform for various postpolymerization modifications.

Synthesis of $A_m(OH)_m$-type (A = PEG) multiarm star by epoxy-carboxyl coupling reaction

Epoxy-based ring-opening reactions were usually used to introduce reactive functionality or form cured system although
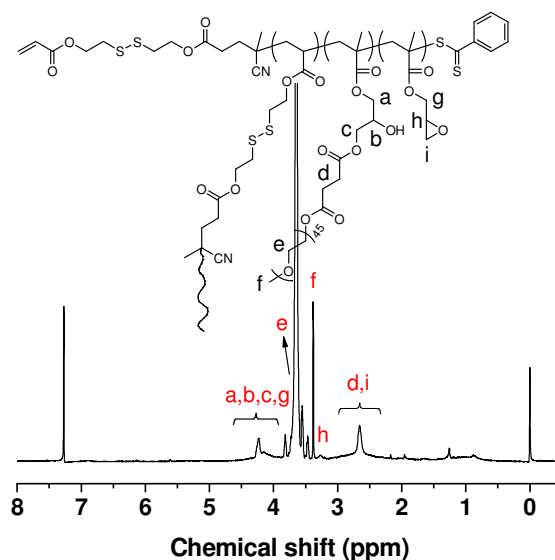
Fig. 3 ^{1}H NMR spectrum of star PEG with a branched core (The wavy line denotes PGMA branches grafted with PEG segments).

they were seldom utilized to bridge various polymeric chains to construct more complex macromolecular architecture. In this study, epoxy-carboxyl coupling reaction between hyperbranched PGMA and MPEG-COOH was used to generate hydroxyl-functionalized $(PEG)_m$ star with a branched core, in which PEG arms were grafted onto the branched substrate via grafting onto approach, and hydroxyl functionality was in-situ generated during the reaction and could be used to grow an alternative arm via "grafting from" approach.

The reaction using PPh$_3$ catalyst ($[MPEG\text{-}COOH]_0$:$[GMA]_0$:$[PPh_3]_0$ = 10:20:0.1) was performed in DMF at 110 °C for 20 h (run 2 of Table 1), and the resultant star PEG was purified by precipitation, dialysis and freeze-drying. GPC and ^{1}H NMR analyses confirmed the absence of unreacted MPEG-COOH in isolated star PEG. The GPC trace only exhibited symmetric

monomodal distribution corresponding to star polymer, and the M_n and PDI values were obtained as 65700 and 1.26 (Fig. 2). In ^{1}H NMR spectrum of MPEG-COOH, the characteristic signals appeared at 4.26 (CH_2OCO) and 2.65 ppm ($OCOCH_2CH_2COOH$).

5 In ^{1}H NMR spectrum of purified star PEG (Fig. 3), the signals of CH_2OCO originating from ring-opening reaction appeared at 4.23 ppm, and other characteristic signals were observed at 3.65 (CH_2CH_2O of PEG), 3.38 (CH_3O of PEG), and 2.66 ppm (CH_2CH_2COO connecting with PEG). As compared with [1]H

10 NMR spectrum of hyperbranched PGMA (Fig. 1), it can be seen the signals of epoxy moieties in star PEG were significantly weakened, and the signal of CHO (epoxy) was noted in 3.27 ppm. Based on the equation $e = I_{3.38}/(I_{3.38} + 3I_{3.27})$, it was estimated 43.7% of GMA units had participated in the epoxy-carboxyl

15 reaction. However, the graft number of PEG ($m = M_n$(star PEG) – M_n(hyperbranched PGMA)/M_n(MPEG-COOH)) was determined as 23.0 according to M_n of 65700, and thus it could deduce about 21.9% of GMA units had reacted with MPEG-COOH. In addition to experimental errors in both GPC and NMR measurements, the

20 higher coupling efficiency estimated by ^{1}H NMR analysis may be ascribed to the potential shielding effect. During the graft process, steric hindrance could prevent MPEG-COOH (DP ≈ 45) from approaching inner epoxy moieties in PGMA branches (RB ≈ 11), and PEG chains were preferentially grafted onto the surface

25 of hyperbranched PGMA. Although PGMA in the hyperbranched polymer could adopt stretching coil conformation, most of GMA units in star PEG exhibited more compact chain conformation due to the presence of longer PEG grafts. The remaining epoxy functionalities were partly shielded by PEG segments and more

30 difficult to be monitored during NMR measurement, and thus ^{1}H NMR analysis was liable to overestimate the coupling efficiency.

Synthesis of A_mB_n (A = PEG, B = PCL) miktoarm star copolymers by ROP

CL polymerization initiated with $(PEG)_m(OH)_m$ (m ≈ 23) star

35 using $Sn(Oct)_2$ catalyst was used to generate epoxy-bearing $(PEG)_m(PCL)_n$ (m ≈ n) star copolymers. As ring-opening polymerization ($[CL]_0:[OH]_0:[Sn(Oct)_2]_0 = x:1:0.2$, $x = 20$-60) was performed in toluene at 110 °C for 20 h, $(PEG)_m(PCL)_n$ stars S1-S3 were obtained (runs 3-5 of Table 1). In ^{1}H NMR spectra

40 (Fig. 4), new signals corresponding to PCL segments appeared at 4.06 (CH_2O), 2.31 (CH_2CO), 1.65 and 1.38 ppm (other CH_2) besides signals of PEG segments at 3.65 (CH_2CH_2O) and 3.38 ppm (CH_3O). By comparing integrated signal areas at 3.65 (CH_2CH_2O of PEG) and 2.31 ppm (CH_2CO of PCL), the

45 polymerization degree of PCL arms ($DP_{PCL} = 90I_{2.31}/I_{3.65}$) by assuming all the hydroxyl functionality had quantitatively initiated the polymerization were calculated as 16.9 (S1), 33.7 (S2) and 58.9 (S3), respectively. The molecular weights ($M_{n,NMR}$) were determined to be within the range of 111-221 kDa by [1]H

50 NMR analysis, which were roughly comparable to M_n given by GPC-MALLS and theoretical values ($M_{n,th}$) calculated from M_n(macroinitiator) and monomer conversion. As compared with star PEG, the GPC traces of S1-S3 completely shifted to higher molecular weight side, with polydispersity indices lower than 1.2.

55 These results confirmed that CL polymerization was efficiently conducted. In case of quantitative initiation, AB-type V-shaped grafts could be grafted onto the surface of hyperbranched PGMA

to form $(AB)_m$-type miktoarm stars. Owing to the signal overlapping between $CHOH$ and $COOCH_2$ and relatively low

60 content of hydroxyl moieties, it was difficult to demonstrate if all the hydroxyl functionality had participated in the polymerization by ^{1}H NMR analysis. Consequently, the target star copolymers with PEG and PCL arms could be efficiently achieved by ROP of CL under optimized conditions.

65 Although tin catalyzed ROP of CL appears to be uncontrolled and leads to increasing polydispersity in some cases, the polydispersity indices of star copolymers obtained in this study are liable to decrease with coupling of PEG and growth of PCL. This phenomenon could be primarily ascribed to the differences

70 in reactivity and macromolecular conformation. During coupling of PEG and CL polymerization, hyperbranched PGMA and star PEG with lower molecular weight were liable to exhibit comparatively high reactivity due to reduced steric hindrance and enhanced probability for MPEG-COOH and CL monomer to

75 approach the reactive sites, and thus the resultant products were of lowered polydispersity than their precursors. On the other hand, with increasing molecular weight and chemical composition, star PEG and $(PEG)_m(PCL)_n$ star copolymers had increasing possibility to adopt globular conformation in THF, and GPC

80 analysis may partly underestimate polydispersity indices due to the potential role of mutual compensation of short and long polymer segments on hydrodynamic volumes.
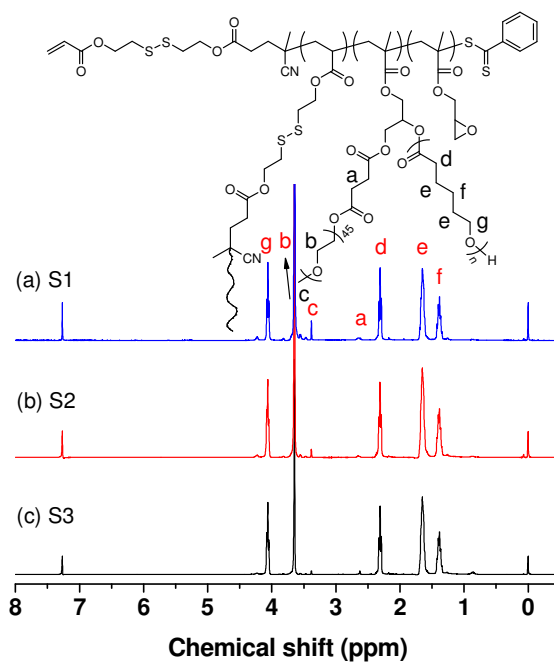
Fig. 4 ^{1}H NMR spectra of $(PEG)_m(PCL)_n$ star copolymers with a

85 branched core (The wavy line denotes PGMA branches grafted with PEG and PCL segments).

Reduction-triggered cleavage of star copolymer

As the disulfide linkages are cleaved, A_mB_n star can be

90 potentially degraded into thiol and epoxy dual-functionalized starlike, comblike and comblike-linear block copolymers (Scheme 2). Starlike (densely grafted) and comblike (loosely

grafted) copolymers comprise PGMA backbone and PEG/PCL segments in which each PGMA branch in A_mB_n star precursor has more or less grafted chains, and block copolymers involve both comblike (polymer brush with PEG and PCL grafts) and linear

5 (originating from ungrafted PGMA branch) blocks. To further understand the microstructure of cleavable copolymers, S2 star (M_n = 150 kDa, DPI = 1.13) was treated with excess Bu$_3$P and subjected to GPC analysis. Owing to the cleavage of disulfide linkages, the molecular weight of the degraded sample was

10 remarkably decreased (M_n = 29800), and the molecular weight distribution was obviously broadened (PDI = 1.30, Fig. 2f). By assuming that the number of disulfide linkages was equal to CTA functionality, there were about 5.2 cleavable moieties in the branched core of star copolymer. Based on ^{1}H NMR analysis,

15 18% of disulfide linkage was connected with the residual acrylic group and 82% of disulfide moiety was located in the branching point (Fig. 1). Theoretically, one star copolymer could be cleaved into about 5.1 copolymers with PEG and PCL segments (f = 6.2 × 82%). The experimental value (M_n(original)/M_n(cleaved) = 5.0)

20 was close to the expected one, revealing the disulfide-linked star copolymer could be efficiently degraded into lower-molecular-weight thiol-bearing copolymers under reductive conditions.

To further understand the effect of reduction-triggered cleavage on overall star structure and types of fragments, S2 and

25 cleaved S2 were subjected to self-assembly in aqueous solution. DLS results revealed S2 aggregates exhibited monomodal distribution in DLS plots with peak size (D_{peak}) of 132 nm, and they had hydrodynamic diameter (D_h) of 109 nm and particle size distribution (PD) of 0.173 (Fig. S1). On the contrary, copolymer

30 aggregates formed by cleaved S2 were of dimodal distribution (D_{peak} = 159 and 300 nm), and their D_h and PD values were 174 nm and 0.365, respectively. TEM images indicated S2 aggregates were necklace-like micelles comprising small spherical micelles, whilst cleaved S2 aggregates were mixtures of normal and large

35 compound micelles with different sizes (Fig. S2). The different morphologies of copolymer aggregates formed by S2 and its cleaved sample could be ascribed to the change in hydrophobic/hydrophilic interactions originating from distinct architecture, molecular weight and end group.

40 **Scheme 2** Illustration for reduction-triggered formation of starlike/comblike (a, d, e) and comblike-linear block (b, c) copolymers with PEG and PCL segments and thiol moieties (labeled with cyan dots)

45
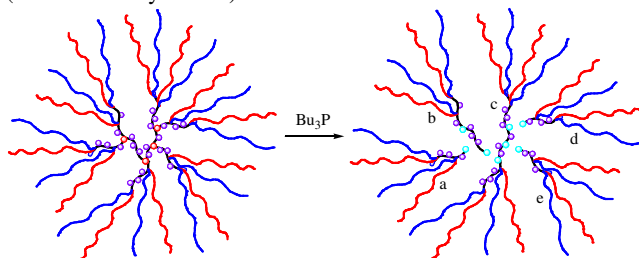
DSC analysis

DSC measurement was performed to understand the glass transition, melting and crystallization behaviors of various polymers. In DSC traces (Fig. 5), one glass transition of

50 hyperbranched PGMA was noted at 56.9 ^{o}C, and the melting

temperature (T_m) of star PEG appeared at 52.5 ^{o}C. The enthalphy of star PEG (ΔH = 89.7 J g^{-1}) was significantly smaller than that of PEG-COOH (ΔH = 137.5 J g^{-1}), revealing the formation of starlike architecture could remarkably reduce the crystallizability

55 of polymer segments. For $(PEG)_m(PCL)_n$ stars, the glass transition ($T_{g,PCL}$) was gradually increased from -52.0 to -49.8 ^{o}C with prolonging PCL, and one or two maximum melting peaks were noted within 40.9 and 54.3 ^{o}C. Different from the sharp melting peak of star PEG, the melting range of star copolymers

60 was obviously broadened possibly due to the differences in crystallization regions and crystalline sizes originating from the highly branched miktoarm architecture. With the introduction of heterogeneous chemical composition and increasing chain length of PCL segments, $(PEG)_m(PCL)_n$ star copolymers were liable to

65 exhibit enhanced topological constraints and hetero-contacts in macromolecular architecture and form crystallization regions with different sizes. Owing to the ability to adjust the formation and percent of homogeneous and heterogeneous crystallization regions and affect degree of crystallization perfection, the chain

70 length ratio of PEG to PCL played important roles in crystallization properties of star copolymers, evident from different melting peaks and enthalphies in DSC traces. PEG was easier to form homogeneous crystallization region than PCL as the chain length of PEG was longer than PCL, and thus the

75 maximum melting peak of S1 was primarily corresponding to the melting of PEG and mixed crystals. Similarly, the maximum melting peak of S2 and S3 could be mainly attributed to the melted PCL and mixed crystals due to the longer chain length of PEG segments. When DP_{PCL} increased from 16.9 to 58.9, the

80 enthalphy was gradually decreased from 79.2 to 48.1 J g^{-1}. It is worth noting that it is difficult to distinguish degree of crystallinity of homogeneous and mixed crystals from each other due to the overlapping of melting peaks and the presence of imperfect crystallization.
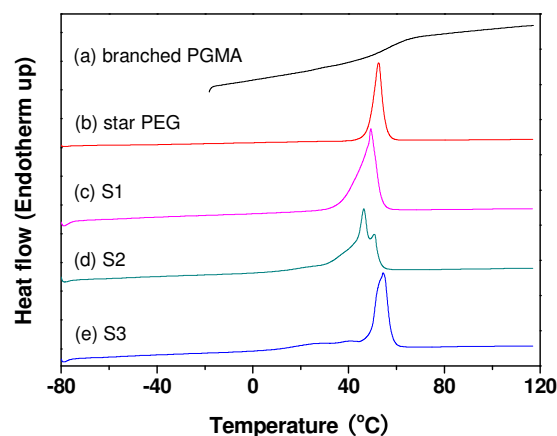
85
**Fig. 5** DSC traces of hyperbranched PGMA, star PEG and $(PEG)_m(PCL)_n$ star copolymers (S1-S3).

Postpolymerization modification of star copolymers via
90 **epoxy-carboxyl/phenol coupling reactions**

The presence of epoxy functionality in star copolymers allows for versatile postmodification due to its high reactivity with sodium

azide, thiol, amine, acid and phenol, and both hydroxyl and an alternative functionality can be obtained by ring-opening reaction. To further introduce some functionalities such as fluorescent and couplable moieties into the side chains of PGMA branches, 7-hydroxy-4-methylcoumarin (C4), 4-oxo-4-(prop-2-yn-1-yloxy) butanoic acid and 2-bromopropionic acid were chosen as model compounds to perform the coupling reaction with epoxy-bearing S3 star. As well documented, coumarin can act as fluorescence marker, alkyne functionality allows for copper(I)-catalyzed azide-alkyne cycloaddition reaction, alkyl bromide is useful for ATRP initiator, azidation and versatile quaternization, and the newly generated hydroxyl functionality can be used for ROP initiator and coupling reaction as well.

Scheme 3 Synthesis of core-functionalized star copolymers with both hydroxyl and coumarin (S4), alkyne (S5) and bromide (S6) moieties (labeled with green dots) via postmodification
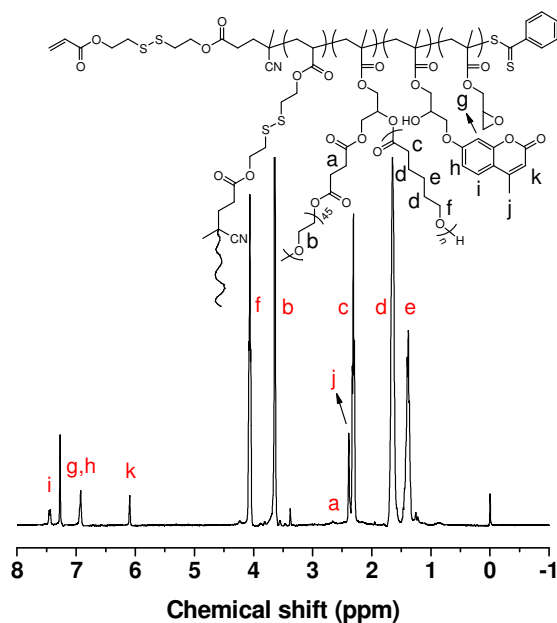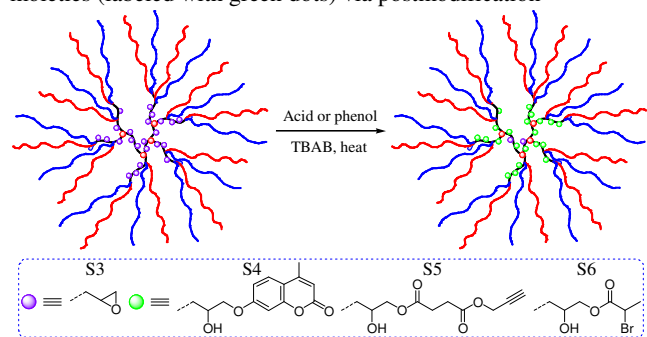
Fig. 6 ^{1}H NMR spectrum of coumarin-functionalized (PEG)$_m$(PCL)$_n$ star (S4, the wavy line denotes PGMA branches grafted with PEG and PCL segments and coumarin moieties).

With the aid of TBAB catalyst, epoxy-carboxyl coupling reaction was conducted in anisole at 100 °C for 30 h, and epoxy-phenol linking reaction was performed in DMSO at enhanced temperature (T = 120 °C) for 20 h due to relatively low reactivity

of phenol moiety in coumarin derivative. After purification, core-functionalized star copolymers with functional groups of coumarin (S4), alkyne (S5) and alkyl bromide (S6) were obtained (Scheme 3). In ^{1}H NMR spectra (Fig. 6 and Fig. S3), the characteristic signals of various functionalities were noted at 7.46 (Ar*H* of coumarin), 6.92 (Ar*H* of coumarin), 6.09 (C*H*COO of coumarin), 2.39 (C*H*$_3$ of coumarin), 4.70 (C*H*$_2$C≡CH), 2.69 (OCOC*H*$_2$C*H*$_2$COO), 2.50 (CH$_2$C≡C*H*), 4.54 (OCOC*H*BrCH$_3$), and 1.83 ppm (OCOCHBrC*H*$_3$), and the signals of epoxy moieties were almost disappeared. By comparing the integrated signal areas of various protons in functional moieties at δ 4.70 (C*H*$_2$C≡CH), 7.46 (Ar*H* of coumarin) and 1.83 (OCOCHBrC*H*$_3$) and PCL segments at 2.31 ppm (C*H*$_2$CO), the coupling efficiency was determined to be higher than 90%. To fully understand the coupling efficiency, coumarin-functionalized S4 star was subjected to GPC-MALLS analysis (M_n = 242000, PDI = 1.16). By comparing the M_n values with S3 star (its precursor), the coupling efficiency was determined to be 97.6%, supporting the afore-mentioned statement on high ring-opening efficiency. In core-functionalized star copolymers, all the functionalities were attached onto the pendant chains of the inner branched core, and thus the coupling efficiency may be partly underestimated owing to the potential shielding effect during ^{1}H NMR measurement. The presence of alkyne, bromide and hydroxyl functionalities in star copolymers allows versatile postmodification reactions in the location of nanosized branched core, which are under way in our group.

Aggregation behaviors and fluorescent properties of coumarin-functionalized star copolymer and its reduction-cleaved sample

The coumarin-based polymers could perform quick photoresponse and effective photoreversibility with alternative irradiation of UV light with different wavelengths,[64–67] and they may exhibit tunable fluorescent behaviors due to the shielding effect to isolate fluorophore and solvent and the restriction in rotation of fluorophores in solution state originating from the rigidness of star or branched molecular scaffolds.[54–57,71,72] Besides construction of core-crosslinked star copolymer as photoresponsive material, coumarin-loaded S4 star is expected to exhibit distinct fluorescence properties in homogeneous and mixed solutions. Considering the potential influence of polymeric architecture and location of fluorophores, the aggregation behaviors and fluorescent properties of S4 star and its reduction-cleaved copolymer (cleaved S4) were investigated in this study.

Although the UV-vis spectra of S4 in THF, water and their mixtures (c = 10 μg mL^{-1}) were roughly similar (Fig. S5), the fluorescence spectra in various solvents were distinctly different (Fig. 7). When excited at 321 nm, the fluorescence spectra of S4 in THF and THF/water mixture with water fraction (f_w) of 10% were similar, and then the fluorescence intensity of S4 solution was liable to increase with increasing water fraction, in which the visible blue light became stronger with gradual addition of water. Meanwhile, a noticeable shift in the maximum emission was noted, and the emission spectra in THF/water mixtures usually exhibited dual or triple fluorescence emission peaks covering the interval of 340-625 nm (Fig. 7). The copolymer solutions ($f_w = 0$ and 10%) had maximum emissions (λ_{em}) at 388 and 498 nm

corresponding to emissions from single molecule and excimer of coumarin moieties. With increasing water fraction, the bands at 388 and 498 nm were gradually weakened, and the intensity at 451 nm increased immediately, in which the coumarin moieties were more isolated from water and the fluorescence spectrum resembled the emission from the donor (O and the neighboring OH) to the acceptor (C=O) of the isolated fluorophore due to intramolecular charge transfer. In THF and mixture with 10% of water, the I_{388}/I_{498} (1.03) and I_{388}/I_{451} (2.45) values were same due to negligible aggregation. As f_w increased from 10 to 100%, the intensity ratio of I_{388}/I_{498} decreased from 1.03 to 0.12, and the I_{388}/I_{451} value reduced from 2.45 to 0.05, in which the drastically decreased intensity ratios could be ascribed to the enhanced aggregation of star copolymer in solution (Fig. S6).
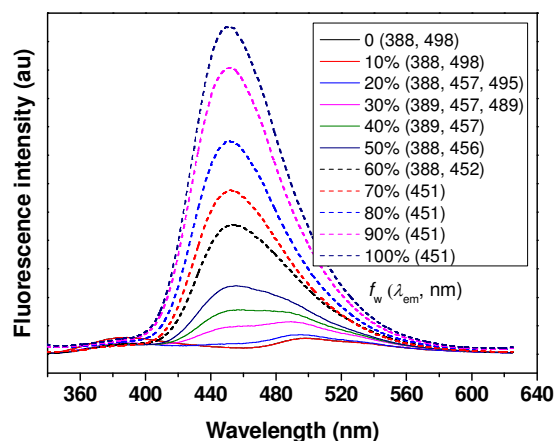

Fig. 7 Dependence of fluorescence spectra of coumarin-functionalized S4 star in THF, water and their mixtures ($c = 10$ µg mL^{-1}, $\lambda_{ex} = 321$ nm) on water fraction, in which water fraction (f_w) and maximum emission (λ_{em}) were listed in the inset.
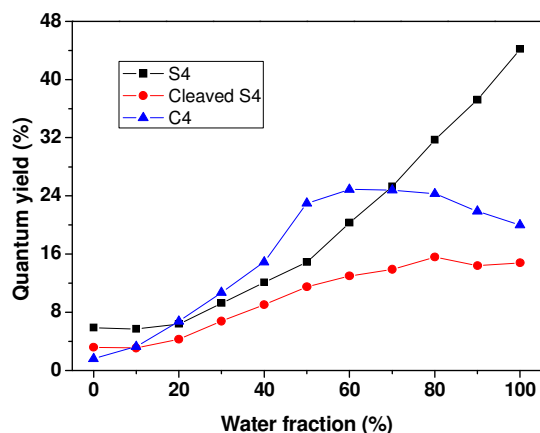
Fig. 8 Influence of water fraction on quantum yields of S4, cleaved S4 ($c = 10$ µg mL^{-1}) and 7-hydroxy-4-methylcoumarin (C4, $c = 5.0$ µg mL^{-1}) in THF, water and their mixtures ($\lambda_{ex} = 321$ nm).

On this basis, the fluorescence quantum yields (Φ_F) of S4 in various solutions were measured (Fig. 8). The Φ_F values only fluctuated between 5.70% and 6.39% ($f_w = 0$-20%) and gradually increased from 9.26% to 44.2% as water fraction varied from 30% to 100%. These results were in good accordance with the evolution of light scattering intensities of S4 solutions. As f_w increased from 10 to 50%, the hydrodynamic diameters (D_h) of S4 aggregates given by DLS measurement continuously increased from 166 to 486 nm (a-e of Fig. 9), and the low derived count rate (DCR) values (3.3-15.7 kcps, $f_w = 10$-20%) immediately jumped to 393-666 kcps ($f_w = 30$-50%, Table S1). Owing to the continuous formation of self-assembled aggregates, light scattering intensities were substantially enhanced with gradual addition of water. When f_w further enhanced to 70-100% (g-j of Fig. 9), the D_h values were fluctuated between 716-754 nm, and no notable change in light scattering intensities was observed (DCR = 1347-1370 kcps). With increasing water fraction, the solvent polarity was liable to increase, and the resultant copolymer aggregates exhibited a wide range of intriguing morphologies (Fig. 10) including micelles ($f_w = 10$-20%), vesicles ($f_w = 30$-50%), large vesicles ($f_w = 60$-90%), and hyperbranched micelles comprising unimolecular micelles ($f_w = 100\%$).
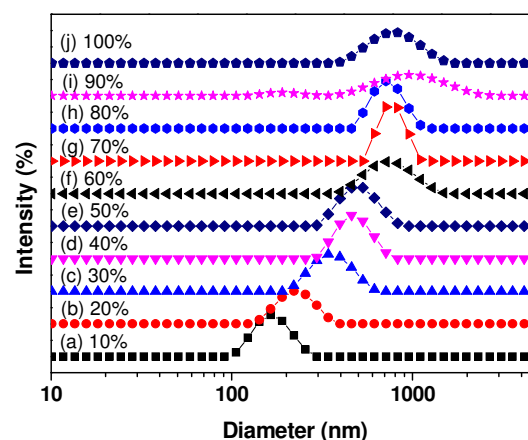
Fig. 9 DLS plots of coumarin-functionalized S4 star in THF–water mixtures or water with various water fraction ($f_w = 10$-100%) and concentration of 10 µg mL^{-1}.

The quantum yields of S4 star were liable to increase with increasing water fraction, which could be primarily attributed to the influence of solvent polarity on microenvironment comprising polymer chains, fluorophores and solvent. In a good solvent ($f_w = 0$ and 10%), most of coumarin moieties could directly interact with the solvent since PEG and PCL chains and the branched core preferentially adopted the stretching conformation, and two bands with peaks at 388 and 498 nm were noted in fluorescence spectra. With gradual addition of water ($f_w = 20$-60%), the hydrophobic PCL segments gradually collapsed, and S4 star was liable to form copolymer aggregates, during which water molecules beside coumarin moieties were gradually pulled out due to the enhanced aggregation behaviors. In this stage, the influence of solvent polarity on fluorophores was increasingly

weakened, and the band with peak at about 452-457 nm emerged and enhanced. As water fraction was beyond 60%, the coumarin groups were surrounded by polymer segments and isolated from the solvent due to the increasing shrinkage of star copolymer, and
5 the rotation of fluorophores was efficiently restricted. Therefore, only a single band at 451 nm corresponding to emission from intramolecular charge transfer appeared in fluorescence spectra as water fraction was high enough.
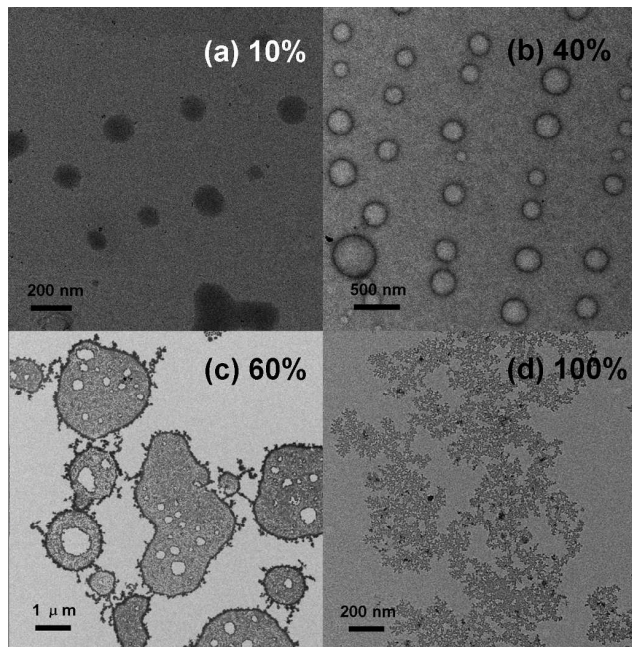
10 **Fig. 10** Typical TEM images of S4 aggregates ($c = 10$ μg mL^{-1}) formed in water and THF/water mixtures with different water fraction.

To reveal the influence of topology and location of coumarin
15 moieties, the aggregation behaviors and fluorescent properties of cleaved S4 obtained by Bu$_3$P triggered degradation were also investigated. As plotted in Fig. S8, the fluorescence spectra of cleaved polymer were strongly dependent on water fraction. The fluorescence spectra of cleaved S4 in THF and mixture with 10%
20 of water were comparable, and the fluorescence intensity gradually increased with an increase in water fraction. The D$_h$ values of cleaved S4 in THF/water mixtures varied between 220 and 474 nm, and the hydrodynamic diameter was around 326 nm in aqueous solution (Fig. S9). The DCR values first increased
25 from 68.8 ($f_w = 10\%$) to 2513 kcps ($f_w = 80\%$) and then dropped to 1586 kcps ($f_w = 100\%$). In the same solvents, S4 star and its reduction-cleaved copolymer had distinctly different D$_h$, particle size distribution (PD) and light scattering intensities (Table S1), revealing the aggregation behaviors could be affected by some
30 factors such as topology, molecular weight and end group. The Φ_F values were calculated within the range of 3.07-15.6% (Fig. 8), in which the quantum yield in THF and mixture with 10% of water was similar, and it increased from 3.07% ($f_w = 10\%$) to 15.6% ($f_w = 80\%$) and then slightly decreased to 14.8% ($f_w =
35 100\%$). The remarkably different fluorescent properties of S4 star and its cleaved copolymer may be attributed to the difference in polymeric topology and the potential quenching ability of thiol moieties in cleaved S4.

The quantum yield of 7-hydroxy-4-methylcoumarin (C4) in
40 THF was 1.62% (Fig. 8), and it increased to 5.87% (S4 star) and 3.17% (cleaved S4) as the coumarin moiety was attached onto the side chain of GMA units. The result was similar to that observed in dendritic molecular brushes[54] and dendrigraft copolymers,[71,72] and the enhanced fluorescence efficiency could be attributed to
45 the steric shielding in the branched architectures which efficiently prevented the fluorophores from self-aggregation and environmental quenching. With increasing water fraction, the quantum yields of C4 initially increased from 1.62% ($f_w = 0$) to 24.9% ($f_w = 60\%$) and then dropped to 20.0% ($f_w = 100\%$), which
50 was potentially ascribed to the differences in solvent polarity and the ability to form hydrogen-bonding interactions.

Careful inspection of the plots in Fig. 8 revealed S4 star was of higher quantum yield than cleaved S4 in same solvents, and the Φ_F(S4 star)/Φ_F(cleaved S4) values were 1.85 (in THF), 3.00
55 (in water) and ranged between 1.29 and 2.58 in THF/water mixtures. These results were primarily ascribed to the differences in the ability to isolate fluorophore and solvent and degree of restricted motion of coumarin moieties in polymer aggregates. In S4 star with architecture similar to the "core-shell" structure, the
60 coumarin groups were attached onto PGMA branches in the inner branched core, and the shielding effect of PEG and PCL segments in the outlayer efficiently prevented the coumarin moieties from intermolecular motion in a good solvent such as THF and THF/water mixture with low f_w. With gradual addition
65 of water, large aggregates with different morphologies were gradually formed, and most of coumarin groups would be isolated from each other with the shrinkage of the branched core. Accordingly, the intramolecular motion of coumarin moieties could be further restricted due to increasingly compact stacking
70 among polymers. For cleaved S4 with V-shaped grafts, however, the coumarin groups were densely grafted onto polymethacrylate backbone, and the polymer underwent directly chain aggregation with addition of water. Although the presence of PEG and PCL segments could partly disturb the intermolecular motion, the
75 coumarin moieties laid in the hydrophobic core or core-shell interface of copolymer aggregates, and the inter- and intramolecular motions of coumarin groups in reduction-cleaved polymer were simultaneously present. Therefore, both topological effect and location of coumarin moieties played important roles
80 in fluorescent properties.

The above-mentioned results revealed S4 star and its reduction-cleaved copolymer had remarkably different aggregation behaviors and fluorescent properties as they were dissolved and dispersed in THF, water and their mixtures. Upon
85 partial reduction of S4 star, the sample obtained is expected to possess fluorescence spectra and quantum yields ranging between S4 star and cleaved S4. Disulfide-linked S4 star can exhibit strong blue light upon excitation at 321 nm, and the fluorescent properties are sensitive to water fraction and reduction stimulus.
90 Owing to solvent polarity and reduction dual-dependent fluorescent properties, S4 star may have a great potential as stimuli-responsive imaging materials in "green" ink, coating and precursors for biomedical applications. The influence of UV irradiation on physicochemical properties is in progress and will
95 be reported later.

Conclusions

$(PEG)_m(PCL)_n$ ($m \approx n \approx 23$) miktoarm stars with a disulfide-linked PGMA branched core were controllably synthesized by combination of RAFT SCVP, epoxy-carboxyl coupling reaction and ROP. The amphiphilic stars obtained were characterized by ^{1}H NMR spectra, GPC-MALLS, DSC and reduction-triggered degradation, and the results fully confirmed the nature of star-branched architecture. The remaining epoxy functionalities in the branched core allowed versatile postpolymerization modification, evident from the efficient introduction of hydroxyl and an alternative functionality such as coumarin, alkyne and alkyl bromide into PGMA branch. Owing to the differences in isolation of fluorophores from solvent and restricted rotation of fluorescent groups in nanosized branched core, coumarin-functionalized star copolymer was liable to exhibit adjustable fluorescent properties in water and THF/water mixtures. The aggregation behaviors and fluorescent properties of coumarin-functionalized polymers were significantly affected by polymeric architecture, location of coumarin moieties and solvent polarity, evident from different physicochemical parameters of S4 star and its reduction-cleaved copolymer in various solutions. Epoxy-based postpolymerization modification further paves ways for facile construction of a wide range of stimuli-cleavable core-functionalized star copolymers with promising applications in imaging, catalysis, host-guest chemistry and biological fields.

Acknowledgements

Notes and references

Suzhou Key Laboratory of macromolecular Design and Precision Synthesis, Jiangsu Key Laboratory of Advanced Functional Polymer Design and Application, College of Chemistry, Chemical Engineering and Materials Science, Soochow University, Suzhou 215123, China. Tel: +86-512-65882045; Fax: +86-512-65882045; E-mail: *ylzhao@suda.edu.cn*

† Electronic Supplementary Information (ESI) available: [^{1}H NMR, IR, UV-vis and fluorescence spectra, DLS plots, and TEM images]. See DOI: 10.1039/ b000000x/

1   N. Hadjichristidis, M. Pitsikalis, S Pispas and H. Iatrou, *Chem. Rev.*, 2001, **101**, 3747–3792.
2   N. Hadjichristidis, H. Iatrou, M. Pitsikalis and J. Mays, *Prog. Polym. Sci.*, 2006, **31**, 1068–1132.
3   H. F. Gao and K. Matyjaszewski, *Prog. Polym. Sci.*, 2009, **34**, 317–350.
4   H. I. Lee, J. Pietrasik, S. S. Sheiko and K. Matyjaszewski, *Prog. Polym. Sci.*, 2010, **35**, 24–44.
5   M. Ouchi, T. Terashima and M. Sawamoto, *Chem. Rev.*, 2009, **109**, 4963–5050.
6   D. J. A. Cameron and M. P. Shaver, *Chem. Soc. Rev.,* 2011, **40**, 1761–1776.
7   A. Gregory and M. H. Stenzel, *Prog. Polym. Sci.*, 2012, **37**, 38–105.
8   K. Kempe, A. Krieg, C. R. Becer and U. S. Schubert, *Chem. Soc. Rev.*, 2012, **41**, 176–191.
9   T. Higashihara, M. Hayashi and A. Hirao, *Prog. Polym. Sci.,* 2011, **36**, 323–375.
10 A. Hirao, R. Goseki and T. Ishizone, *Macromolecules,* 2014, **47**, 1883–1905.
11 Z. B. Li, E. Kesselman, Y. Talmon, M. A. Hillmyer and T. P. Lodge, *Science,* 2004, **306**, 98–101.
12 Z. B. Li, M. A. Hillmyer and T. P. Lodge, *Langmuir,* 2006, **22**, 9409–9417.
13 N. Saito, C. Liu, T. P. Lodge and M. A. Hillmyer, *Macromolecules,* 2008, **41**, 8815–8822.
14 C. Liu, M. A. Hillmyer and T. P. Lodge, *Langmuir,* 2009, **25**, 13718–13725.
15 N. Saito, C. Liu, T. P. Lodge and M. A. Hillmyer, *ACS Nano,* 2011, **4**, 1907–1912.
16 A. O. Moughton, M. A. Hillmyer and T. P. Lodge, *Macromolecules,* 2012, **45**, 2–19.
17 W. Kong, B. Li, Q. Jin, D. Ding and A.-C. Shi, *J. Am. Chem. Soc.*, 2009, **131**, 8503–8512.
18 A. Hanisch, A. H. Gröschel, M. Förtsch, M. Drechsler, H. Jinnai, T. M. Ruhland, F. H. Schacher and A. H. E. Müller, *ACS Nano,* 2013, **7**, 4030–4041.
19 K. Khanna, S. Varshney and A. Kakkar, *Polym. Chem.,* 2010, **1**, 1171–1185.
20 D. Kuckling and A. Wycisk, *J. Polym. Sci. Part A: Polym. Chem.*, 2013, **51**, 2980–2994.
21 A. A. Steinschulte, B. Schulte, N. Drude, M. Erberich, C. Herbert, J. Okuda, M. Möller and F. A. Plamper, *Polym. Chem.*, 2013, **4**, 3885–3895.
22 K. Y. Baek, M. Kamigaito and M. Sawamoto, *Macromolecules,* 2001, **34**, 215–221.
23 J. H. Xia, X. Zhang and K. Matyjaszewski, *Macromolecules,* 1999, **32**, 4482–4484.
24 H. F. Gao and K. Matyjaszewski, *Macromolecules,* 2006, **39**, 3154–3160.
25 J. Ueda, M. Kamigaito and M. Sawamoto, *Macromolecules,* 1998, **31**, 6762–6768.
26 Y. L. Zhao, X. T. Shuai, C. F. Chen and F. Xi, *Macromolecules,* 2004, **37**, 8854–8862.
27 Y. L. Zhao, Y. M. Chen, C. F. Chen and F. Xi, *Polymer,* 2005, **46**, 5808–5819.
28 H. F. Gao and K. Matyjaszewski, *Macromolecules,* 2006, **39**, 4960–4965.
29 M. R. Whittaker, C. N. Urbani and M. J. Monteiro, *J. Am. Chem. Soc.,* 2006, **128**, 11360–11361.
30 J. Z. Du and Y. M. Chen, *Macromolecules,* 2004, **37**, 3588–3594.
31 Y. L. Zhao, T. Higashihara, K. Sugiyama and A. Hirao, *J. Am. Chem. Soc.*, 2005, **127**, 14158–14159.
32 T. Higashihara, M. Nagura, K. Inoue, N. Haraguchi and A. Hirao, *Macromolecules,* 2005, **38**, 4577–4587.
33 C. N. Ye, G. D. Zhao, M. J. Zhang, J. Z. Du and Y. L. Zhao, *Macromolecules,* 2012, **45**, 7429–7439.
34 K. Hamilton and S. Perrier, *J. Polym. Sci. Part A: Polym. Chem.,* 2009, **47**, 6396–6408.
35 A. Nese, J. Mosnáček, A. Juhari, J. A. Yoon, K. Koynov, T. Kowalewski and K. Matyjaszewski, *Macromolecules,* 2010, **43**, 1227–1235.
36 X. Jiang, M. J. Zhang, S. X. Li, W. Shao and Y. L. Zhao, *Chem. Commun.,* 2012, **48**, 9906–9908.
37 C. Y. Hong, Y. Z. You, J. Liu and C. Y. Pan, *J. Polym. Sci. Part A: Polym. Chem.*, 2005, **43**, 7379–6393.
38 M. Jesberger, L. Barner, M. H. Stenzel, E. Malmström, T. P. Davis and C. Barner-Kowollik, *J. Polym. Sci. Part A: Polym. Chem.,* 2003, **41**, 3847–3861.
39 C. B. Zhang, Y. Zhou, Q. Liu, S. X. Li, S. Perrier and Y. L. Zhao, *Macromolecules,* 2011, **44**, 2034–2049.
40 M. J. Zhang, H. H. Liu, W. Shao, C. N. Ye and Y. L. Zhao, *Macromolecules,* 2012, **45**, 9312–9325.
41 J. Han, S. P. Li, A. J. Tang and C. Gao, *Macromolecules,* 2012, **45**, 4966–4977.
42 J. M. J. Fréchet, M. Henmi, I. Gitsov, S. Aoshima, M. R. Leduc and R. B. Grubbs, *Science,* 1995, **269**, 1080–1083.

43 K. Matyjaszewski, *Macromolecules,* 2012, **45**, 4015–4039.

44 M. Rikkou-Kalourkoti, K. Matyjaszewski and C. S. Patrickios, *Macromolecules,* 2012, **45**, 1313–1320.

45 K. Matyjaszewski and N. V. Tsarevsky, *J. Am. Chem. Soc.,* 2014, **136**, 6513–6533.

46 C. Pugh, A. Singh, R. Samuel and K. M. B. Ramos, *Macromolecules,* 2010, **43**, 5222–5232.

47 S. Muthukrishnan, G. Jutz, X. André, H. Mori, and A. H. E. Müller, *Macromolecules,* 2005, **38**, 9–18.

48 K. T. Powell, C. Cheng and K. L. Wooley, *Macromolecules,* 2007, **40**, 4509–4515.

49 J. Chiefari, Y. K. Chong, F. Ercole, J. Krstina, J. Jeffery, T. P. T. Le, R. T. A. Mayadunne, G. F. Meijs, C. L. Moad, G. Moad, E. Rizzardo and S. H. Thang, *Macromolecules*, 1998, **31**, 5559–5562.

50 Z. M. Wang, J. P. He, Y. F. Tao, L. Yang, H. J. Jiang and Y. L. Yang, *Macromolecules,* 2003, **36**, 7446–7452.

51 A. P. Vogt and B. S. Sumerlin, *Macromolecules,* 2008, **41**, 7368–7373.

52 M. J. Zhang, H. H. Liu, W. Shao, K. Miao and Y. L. Zhao, *Macromolecules,* 2013, **46**, 1325–1336.

53 S. P. Li, J. Han and C. Gao, *Polym. Chem.,* 2013, **4**, 1774–1787.

54 S. P. Li and C. Gao, *Polym. Chem.*, 2013, **4**, 4450–4460.

55 J. Liu, J. W. Y. Lam and B. Z. Tang, *Chem. Rev.*, 2009, **109**, 5799–5867.

56 R. R. Hu, N. L. C. Leung and B. Z. Tang, *Chem. Soc. Rev.*, 2014, **43**, 4494–4562.

57 J. Mei, Y. N. Hong, J. W. Y. Lam, A. J. Qin, Y. H. Tang and B. Z. Tang, *Adv. Mater.,* 2014, **26**, 5429–5479.

58 M. Beija, M.-T. Charreyre and J. M. G. Martinho, *Prog. Polym. Sci.,* 2011, **36**, 568–602.

59 A. M. Breul, M. D. Hager and U. S. Schubert, *Chem. Soc. Rev.,* 2013, **42**, 5366–5407.

60 A. A. Steinschulte, B. Schulte, S. Rütten, T. Eckert, J. Okuda, M. Möller, S. Schneider, O. V. Borisovdef and F. A. Plamper, *Phys. Chem. Chem. Phys.,* 2014, **16**, 4917–4932.

61 A. A. Steinschulte, B. Schulte, M. Erberich, O. V. Borisov and F. A. Plamper, *ACS Macro Lett.*, 2012, **1**, 504–507.

62 E. Blasco, B. V. K. J. Schmidt, C. Barner-Kowollik, M. Piñol and L. Oriol, *Macromolecules*, 2014, **47**, 3693–3700.

63 G. M. Soliman, R. Redon, A. Sharma, D. Mejía, D. Maysinger and A. Kakkar, *Macromol. Biosci.*, 2014, **14**, 1312–1324.

64 J. Q. Jiang, B. Qi, M. Lepage and Y. Zhao, *Macromolecules,* 2007, **40**, 790–792.

65 Y. Zhao, *Macromolecules,* 2012, **45**, 3647–3657.

66 J. F. Gohy and Y. Zhao, *Chem. Soc. Rev.*, 2013, **17**, 7117–7129.

67 J. Q. Jiang, Q. Z. Shu, X. Chen, Y. Q. Yang, C. L. Yi, X. Q. Song, X. Y. Liu and M. Q. Chen, *Langmuir,* 2010, **26**, 14247–14254.

68 Y. Shao, C. Y. Shi, G. F. Xu, D. D. Guo and J. T. Luo, *ACS Appl. Mater. Interfaces,* 2014, **6**, 10381–10392.

69 M. Spiniello, A. Blencowe and G. G. Qiao, *J. Polym. Sci. Part A: Polym. Chem.*, 2008, **46**, 2422–2432.

70 J. Q. Jiang, Y. Liu, Y. H. Gong, Q. Z. Shu, M. Yin, X. Y. Liu and M. Q. Chen, *Chem. Commun.*, 2012, **48**, 10883–10885.

71 Y. Zhang, K. H. Shen, F. Guo, Y. F. Wang, Y. S. Wang, Y. R. Wang and Y. Li, *RSC Adv.,* 2013, **3**, 20345–20352.

72 Y. Zhang, F. Guo, K. H. Shen, Y. Y. Ren and Y. Li, *Polymer,* 2014, **55**, 1202–1208.

73 Y. Mitsukami, M. S. Donovan, A. B. Lowe and C. L. McCormick, *Macromolecules,* 2001, **34**, 2248–2256.

74 L. Tao, J. Q. Liu, J. B. H. Tan and T. P. Davis, *Macromolecules,* 2009, **42**, 4960–4962.

75 X. T. Shuai, Z. Jedlinski, Q. Luo and N. Farhod, *Chin. J. Polym. Sci.,* 2000, **18**, 19–23.

76 Y. Zhang, H. K. He and C. Gao, *Macromolecules,* 2008, **41**, 9581–9594.